International Journal of Engineering Trends and Technology
ISSN: 2231 – 5381 / https://doi.org/10.14445/22315381/IJETT-V70I6P238
Volume 70 Issue 6, 379-394, June 2022

Original Article

Bacterial Foraging and Seagull Optimization Algorithm based THD level Comparison for Flyback Converter in Grid-connected PV System

C Sunil Kumar[1], Puttamadappa C[2], Y L Chandrashekar[3]

[1]*Electrical & Electronic Engineering, PES College of Engineering, Mandya, Karnataka, India*
[2]*Electronics & Communication Engineering, Dayananda Sagar University, Bangalore, Karnataka, India*
[3]*Electronics & Communication Engineering, Mysore Royal Institute of Technology, Mandya, Karnataka, India*

[1]*suteju23@gmail.com*

Received: 11 April 2022 Revised: 03 June 2022 Accepted: 15 June 2022 Published: 30 June 2022

Abstract *- With intensifying integration of grid and photovoltaic (PV) systems, the power quality (PQ) is a prime constraint in modern power systems. Here, the reactive and active power controller is bid with a three-phase grid integrated PV system to magnify the PQ based on the Seagull Optimization Algorithm (SOA). The proposed system comprises two key controllers: the Flyback converter with Bacterial Foraging Optimization Algorithm (BFOA) to track the utmost powers from the PV panels and the suggested SOA optimized controller for the grid-integrated three-phase inverter. The integration of grid and PV utilizes a three-phase modular multilevel inverter (MMI) that manages the active and reactive powers by optimizing the SOA controller using the grid side voltage. The proposed control strategy minimizes power dropping into the inverter by regulating the instantaneous active and reactive powers to improve PQ. Moreover, it can reduce the harmonic and compensate for reactive power. The simulation of the proposed system is by utilizing the MATLAB/Simulink platform, and its outcomes are analyzed and equated with previously generated methods. The proposed methodology is compared with the conventional methods like Atom Search Algorithm (AOA), Grey Wolf Optimization (GWO), GSA, and GA, respectively.*

Keywords *- Active and reactive power controller, Grid-connected PV system, Gravitational Search Algorithm (GSA), Genetic Algorithm (GA), SOA and BFOA*

1. Introduction

Emerging concerns over the environment and energy independence have led to expanding the perception of renewable energy systems in power networks [1]. Since it is easy to install and involves low maintenance costs, the solar PV system is becoming more evident [2]. On that account, the PV system has become a revolutionary power generation source in the present and forthcoming years [3]. The electrical energy is generated through PV arrays, and that energy is within easy reach of the communal use by grid-connected PV systems [4]. Generally, it turns all radiation absorbed into active power and ignores the generation of reactive power [5]. The converters are the primary components of grid-integrated VSI, which transfer power with DC-AC [6]. It takes in to adjust the dc-link voltage and handle the power flow in the middle of the PV generator and grid is common [7].

Besides voltage deviations generated by the rate of total harmonic distortion (THD), power factor and voltage fluctuations, and other standards are comprised in the PQ. Furthermore, the PV inverter can also be optimized under a certain control strategy [8]. In addition, the grid voltage in inclusion goes through PQ problems of under-voltage, over-voltage, and harmonics on account of unstable and non-linear loads [9]. Various researches in the power quality field development as reactive power compensation, power generation, and solar energy conversion system by harmonic filtering are described in the literature [10]. To minimize the power loss in the grid line, the PV inverter entirely transformed the PV inverter into a static reactive power generator by utilizing the control strategy [11]. To eliminate harmonics in the grid, an adaptive current control strategy utilized the Proportional Resonant (PR) controller for PV inverters [12]. A power angle control method was presented for decreasing the grid side THD in the PV system. Moreover, it improves the power factor and reactive power compensation [13]. Another control method is attaining certain power attributes like active/reactive power ripple, and THD of the output current was evolved with adjustable power quality attributes [14].

The Single-stage DC–AC converter systems (SSCSs) control pattern in the adapter/converter is used to pass maximum PV power among reactive power controllers [15]. The instantaneous reactive power theory uses the current source inverter (CSI) to put down harmonic currents and reactive power compensation by using the hysteresis current controller [16, 17]. The FLC for utilizing in boost control of PV connected grid system via Z-source inverter was evaluated [18]. The single-phase energy is stored quasi-Z-source cascaded H-bridge (ES-qZS-CHB) inverter PV system to carry through the power control [19, 20]. As a result, a highly dynamic controller is developed to arrange the PV inverter power of the grid directly**.**

2. Recent Research Works: An Overview

To obtain power control in a grid-connected PV model, several techniques are established by some researchers that are reviewed below,

Muhammad Talha *et al.* [21] presented the grid-connected PV inverter installed at the low voltage distribution grid. In architecture, the robustness against faults and operation of the inverter was considered. The robustness against grid faults and operation of the inverter in architecture. The control strategy prevented the inverter from shut down by managing the DC-link. An inverter supports the grid through reactive power injection during the voltage sags. The appropriate references could generate by predictive control for both LVRT and regular Mode. It is based on regulatory grid codes and a two-stage voltage-source-inverter's specification.

Muammar Zainuddin *et al.* [22] have proposed the PQ issues in the grid interconnected PV inverters by injecting the active power. The statistical outcomes of the power quality parameters analyzed in that study, and the parameters are current harmonic components and inverter voltage at different loads, THD on current and voltage, and the changes in relative and reactive power. The VAR regulation used to assess the PQ parameters depends on a constant power factor (CPF).

Preetha Roselyn *et al.* [23] have projected a fuzzy-based reactive and active power control of inverter during grid faults. Based on fuzzy logic, the grid voltage was stabilized by a modified inverter real and reactive power control strategy. For managing the reactive power, the P-Q capability curve of the grid-integrated PV system (GIPV) was derived by improved mathematical methodology proposed by Manash Kumar Mishra and Vivek Nandan Lal [24] at MPP conditions for different ecological situations. By obtaining reactive power limits of a utility-scale single-stage three-phase PV system linked to the distribution grid, this methodology was used by analyzing all the possible sets of working points within the steady area of operation. A PV system was chained with the system controls reactive powers by regulating the voltage of a bus have presented by Insu Kim and Ronald G.Harley[25]

This generic assessment shows that grid-tied three-phase inverters intend to gain high efficiency, excellent performance, and reliability. Multiple difficulties have been experienced while implementing and solving the problems. Some innovations have been found. Due to the growth of renewable energy sources, innovations like grid-tied three-phase inverters received more prominence. Also, various research studies have concentrated on grid-tied inverter control. The PR, PID, and PI controllers handle the grid-tied inverters.

Nevertheless, the PI and PID controller can never eliminate steady-state error for sinusoidal signals. The struggle of PI controllers is tuning gains with variations in atmospheric situations. Even if the reference values are changed suddenly, traditional PI controllers are affected by large overshoots and slow responses. Additionally, the response time of the traditional PI technique was enhanced by a modified structure of PI control. But, in output powers, these approaches generate large fluctuations at a steady state. A back-stepping method is implemented to control the real and reactive output power. The response of this approach is better than the traditional PI control technique because it independently regularizes the real and reactive output powers. However, reducing oscillations in the output powers doesn't provide any effective technique. Even though to trace sinusoidal signals, the PR controller has the capability without steady-state errors. The frequency deviation of the selected harmonic element greatly disturbed the control performance. In non-linear systems, the effective controller removes these negative effects based on a variable structure control strategy.

On the other hand, undesirable chattering in currents occurs when the system is under control. Hence, the direct power control (DPC) used a sliding mode scheme to eliminate this disadvantage. The unpredictable switching frequency generated an unwanted large band gap harmonic spectrum series in this method. It is one of the important drawbacks of that approach. Therefore, a sliding mode direct power control (SMCDPC) with a low crackling level and no extra current loop was proposed. In atmospheric conditions, predictive controllers also cannot appropriately equal changes. The critical task of sliding-mode controllers is time-varying surface selection. However, it is important to fine-tune the gain parameters. Another complex algorithm is needed, such as a meta-heuristic or soft computing technique.

3. Description and Modeling of Proposed System

The proposed power system consists of a PV array, DC-DC converter, proposed controller, and a three-phase grid for distinguishing and investigating the PV system's active and reactive power behavior.

The proposed configuration is shown in figure 1, which illustrates two stages. The first stage is a flyback converter for controlling the maximum threshold power from the PV generator using BFOA based MPPT algorithm. The second stage is a grid-integrated three-phase MMI with a DC link, which is connected to the output of the flyback converter. Insulated Gate Bipolar Transistor (IGBT) legs combined in the three-phase MMI. The R, L filter is connected to resultant terminals of MMI, and the common point of interconnection is linked to the other end of the filter. However, the control stage of the proposed system is implemented into the proposed controller, which concurrently takes care of both aspects.

A sinusoidal command signal is attained based on the maximum PV power and instantaneous load reactive power with the modified p-q principle to implement the proposed control scheme. The topmost power value attained through BFOA-based MPPT is utilized as the source power. Hence, the dc-link voltage is continued as per the highest power distributed by the PV array. In this proposed methodology, the PV is managed with the help of the BFOA algorithm. In this proposed methodology, power quality mitigation is also achieved with the help of the SOA algorithm.

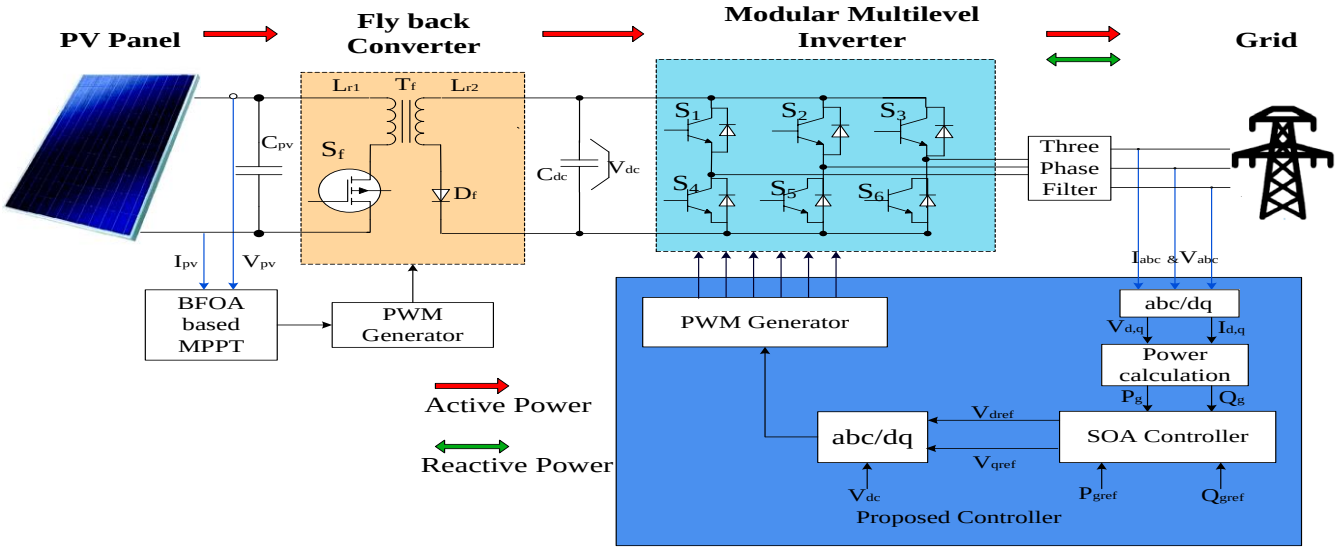

Fig. 1 The system architecture of the proposed Grid-connected PV system

Moreover, the reactive power requested by the grid is reactive reference power. The portion of triggered power through the PV system is reactive power distributed to the grid and conditioned through an inverter. The portion of triggered power through the PV system is reactive power distributed to the grid and conditioned through an inverter. In such a way, those reactive and active current attributes are independently produced to deliver active and reactive power demand.

The storage capacitor is utilized to electronic interchange power and stabilize PV output voltage. A three-phase grid, PV array, and an inverter are comprised of the system. Many PV cells are comprised of the PV array. It is subjected to the sun's radiation, creates possible variance, and supplies voltage to the inverter. Based on the MPPT algorithm, the PV array brings forth the BFOA along with PV voltage and current. Then the algorithm is developed an V_{dc} nd provides the MPP. Then it is streamed via a constant value chooser. If there is low solar radiation and the V_{dc} is low, then a constant value is given so that the grid acquires the continuous power supply. The gating pulses are supplied to the inverter with PWM generator support. Then it provides the current to the grid. The control unit is needed because when a PQ issue occurs, the PV generator connected could connect the PV generator to the grid, and the inverter should inject reactive power. Therefore, the proposed approach followed controlling must be enhanced to enhance the proposed approach followed in controlling to ignore the PV power waste and especially normalize the grid-tied PV system. In this case, the PQ issues are noted when the proposed system control is designed and arranged to switch from common to grid faulty operating Mode. Here the inverter infuses reactive power depending on time duration and PQ level. A three-phase filter smoothens the inverter's resultant voltage for a grid-connecting reactor. The PV array layout and modeling are presented in the followed section.

3.1 Proposed PV Array system

PV systems' robustness problem for parameter uncertainty can be minimized by combining them with other energy sources. To improve the entire system, the inactive

response of a PV can be improved. It provides a constant and continuous power supply to a DC bus. To invert the DC voltage into three-phase AC, an MMI is connected. It is further connected to the grid.

Moreover, non-linear and linear loads are linked to PCC. A filter is linked at the PCC to compensate for the current and source voltage. It provides quality power to the grid. In a module (panel), numerous PV cells are connected in various series and parallel circuits to get power. To produce voltage and current, the groups of PV modules are electrically connected in a parallel series. The PV cells are connected in series and parallel to create an array.

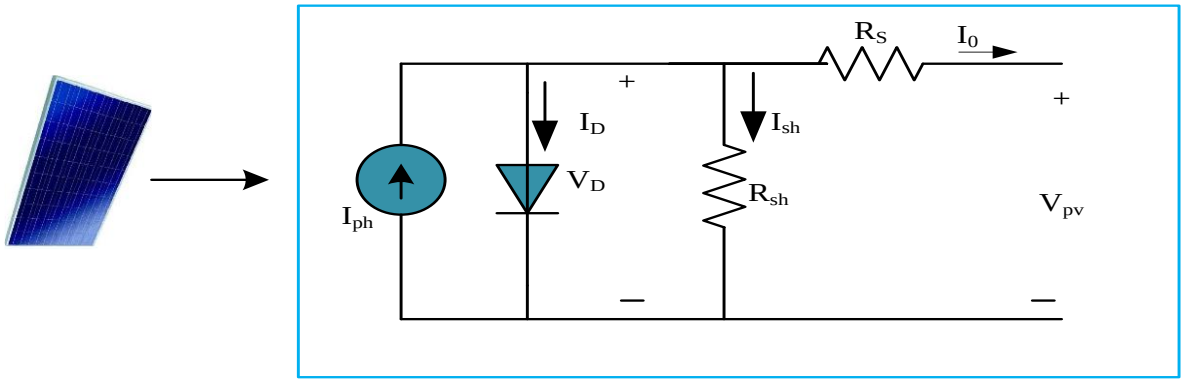

Fig. 2 The equivalent diagram of PV cell

As shown in Fig. (2), in this PV array model, a PV cell is illustrated with one diode and parallel and series resistors by a current source. Equation (1) represents the general current equation,

$$I = I_{pv}^{cell} - I_o^{cell}\left[\exp\left(\frac{qv}{akT}\right)-1\right] \qquad (1)$$

Where I_{pv}^{cell} is the current produced by the incident light, directly proportional to sun irradiation, I_o^{cell} is the diode's leakage current, the electron charge is given as q, Boltzmann constant is k, T is the PN junction temperature, and diode ideality factor constant is denoted a. The interface between n-type and p-type silicon is used to make contact. Holes (p-type) and free electrons (n-type) cancel each other at this coupling point and create a depletion area like a non-conductive barricade. Even though a PV panel comprises several PV cells bound in parallel and series, it also adds certain parameters to the basic equation. Equation (2) represents the modified equation,

$$I = I_{pv} - I_o\left[\exp\left(\frac{V+R_SI}{V_ta}\right)-1\right]-\frac{V+R_SI}{R_p} \qquad (2)$$

And the V_t is given as equation (3),

$$V_t = \frac{N_sKT}{q} \qquad (3)$$

Here, the total number of cells connected in series is given N_s. An experimental PV array contains many other PV modules connected and established by solar cells linked in parallel and series [26]. As a consequence, it represents a single PV panel that is modified into a PV array as equation (4),

$$I = N_{pp}I_{pv} - N_{pp}I_o\left[\exp\left(\frac{N_{ss}V+R_sI\left(N_{ss}/N_{pp}\right)}{V_taN_{ss}}\right)-1\right]-\frac{VN_{ss}+R_sI\left(N_{ss}/N_{pp}\right)}{R_p\left(N_{ss}/N_{pp}\right)} \qquad (4)$$

Here N_{pp} N_{ss} are the total number of PV modules connected in parallel and series. The power produced by the PV is computed by sun radiance and temperature, which is given as equation (5),

$$P_{pv} = P_{pv}^{norm}\eta_{pv}\frac{I_{pv}}{I^{norm}}\left(1+T^{rated}+T_{pv}C^{temp}\right) \qquad (5)$$

In equation (6), the power produced from the group of PV panels is computed.

$$P_{pv}^{total} = \eta_{pv}P_{pv} \qquad (6)$$

Here, the analyzed PV modules are assumed to be attached to a power point tracking device. The generation of a PV system is increased by up to 30%. Due to this, it has become more convenient economically, particularly in an off-grid hybrid system.

3.2. A series connection with a PV panel and output of the DC-DC converter

In the circuit, a single inductance is used by the non-isolated boost converter to increase the voltage of the input. It is within reach to roughly match voltage compared to the conventional converter. The circuit structure is easily accessible and compact because the PWM duty cycle is changed to limit the voltage. But, the panel-rated power should be less than the estimated power of this converter. The overall conversion efficiency is similar to this system's boost converter efficiency. Therefore the required voltage is

greater than the output voltage of a PV panel; some variation often occurs here between the required output voltage of the system and the output voltage of the PV panel.

Moreover, the proposed system can attain the essential output voltage only if the voltage variations are included along with the PV panel's output voltage. This theory was also used in a single PV array [27]. The PV panel's output voltage is associated with the output capacitor of a flyback converter. The output voltage is described by equation (7).

$$V_{dc} = V_c + V_{pv} \tag{7}$$

Here V_c is the flyback converter output, V_{pv} the PV panel voltage, and V_{dc} the output voltage. A small power rating provides only the voltage difference between the output voltage of the PV panel with the isolated flyback converter and the needed voltage. There is no necessity for a flyback converter to generate the complete essential voltage. Therefore, the flyback converter's required power capacity is drastically decreased. The great variation between the output voltage of the PV panel and the required output voltage is higher than the converter's power. At the highest operating point of temperature and supreme irradiation, a converter's highest power point is reached. The converter's maximal power requirement is described in equations (8) and (9),

$$I_{con}^{\max} = \frac{P_{pv}^{temp}}{V_{dc}} \tag{8}$$

$$P_{con} = I_{con}^{\max}\left(V_{dc} - V_{pv}^{temp}\right) = V_{pv}^{temp}\left(\frac{V_{dc} - V_{pv}^{temp}}{V_{dc}}\right) \tag{9}$$

Here V_{pv}^{temp} is the utmost operating temperature of PV module output voltage and P_{pv}^{temp} is the highest operating temperature of PV panel output power. The converter mainly affects the total efficiency. The efficiency of the proposed converter is given in equation (10),

$$\eta_c = \left(P_b + P_c \times \eta_{dc-dc}\right) \times 100 \tag{10}$$

Here, η_c the proposed topology converter efficiency P_b is the bypass power percentage, P_c is the converter power percentage, and η_{dc-dc} denotes the isolated flyback converter's efficiency. To increase the maximum power from PV, the BFOA-based MPPT algorithm helps explain the following section.

3.3. BFO-based MPPT algorithm for maximum power generation

The BFO algorithm describes the E.coli foraging process. Swarming, chemotaxis, reproduction, and elimination-dispersal operations are a few methods [28]. These given four operations are detailed, elaborated, and introduced as follows.

In this phase, the bacterial foraging strategy is replicated. In the beginning, the bacteria will take some time to change its present direction. Bacteria make an effort to move a step ahead after that. The bacterium swims unvarying in the same direction if they find rich nutrients. According to the theory, the optimization domain θ is the position of a bacterium and $\theta_i(j,k,l)$ means the i^{th} bacterium in the j^{th} chemotaxis, k^{th} reproduction, l^{th} and elimination-dispersal procedure. The tumbling definition is described below in equation (11),

$$\varphi(i) = \frac{\Delta(i)}{\sqrt{\Delta(i)^T \Delta(i)}} \tag{11}$$

Here random vector is expressed $\Delta(i); i = 1,2,..., S$. Every element $\Delta_m(i); m = 1,2,..., p$ $\Delta(i)$ is a non-specific number within -1 and 1 for i^{th} the bacterium. The total number of bacteria is denoted as S , and the bacterial position is formulated as equation (12),

$$\theta_i(j+1,k,l) = \theta_i(j,k,l) + C(i)\varphi(i) \tag{12}$$

Here, for i^{th} the bacterium, it $C(i); i = 1,2,..., S$ is a moving step size of the tumble. This characteristic imitates signaling cell to cell. The bacteria emit chemical substances only if they find a lump of nutrients; this chemical emission is to entice other bacteria [29]. If the bacterium is at risk, they will swing to repel one another. This social characteristic is Fig.d as equation (13),

$$J^{cc}(\theta,\theta_i(j,k,l)) = \sum_{i=1}^{S} -d^{att}\exp\left(-w^{att}\sum_{f=1}^{p}\left(\theta^f - \theta_i^f\right)^2\right) + \sum_{i=1}^{S} -h^{rep}\exp\left(-w^{rep}\sum_{f=1}^{p}\left(\theta^f - \theta_i^f\right)^2\right) \tag{13}$$

Here, $\theta = \left[\theta_1, \theta_2, \ldots, \theta_p\right]^T$ it is a bacterium in the optimization θ_i^f domain and is the f^{th} element of the i^{th} bacterium position θ_i (for better understanding, we avoid certain indices). $J^{cc}(\theta,\theta_i(j,k,l))$ Value is the cell-to-cell imparting value that will append with the output in the chemotaxis part j of the fitness function p and the total number of problem dimensions. The contrasting coefficients $d^{att}, w^{att}, h^{rep}$ w^{rep} will indicate the power of attraction or repulsion. According to the fitness value of i^{th} bacterium of the swarming effect is described as equation (14),

$$J(i,j,k,l) = J(i,j,k,l) + J^{cc}(\theta,\theta_i(j,k,l)) \tag{14}$$

A replication step is taken after the step of N^c chemotactic. Let's imagine that even a positive integer is S .

The total member population is S^r who have adequate nourishment so that they will replicate (splits into two) without transformation, which is presented as equation (15),

$$S^r = \frac{S}{2} \tag{15}$$

Their collected costs symbolize the health of a bacterium. If the accumulated cost of the bacterium is high, it lacks proper nutrition for forging in its lifetime. Thus, this bacterium is unhealthy, and the possibility of reproduction is too low. Bacteria are sorted depending on their health in descending order in this stage. Then the S^r unhealthy bacteria perish, and the remaining S^r nutritious bacteria divide into two bacteria in the corresponding locations.

Few bacteria pass away as the environment is unpleasant, e.g., a temperature rise may also hurt a chunk of bacteria. This activity imitates the dispersal of a few bacteria with less elimination probability P^{ed}. At the same time, new bacteria reproduce randomly for replacement. This control process of reactive and active power is explained below topics.

3.4 Actual and Reactive Power Control and Management Strategies

According to the conventional method, frames that rotate synchronously are requested for calculating the reactive power (d-q). If the circuits contain three phases, the voltage and current are shifted into a frame that rotates synchronously. To rectify the negative and harmonics attributes, the Clarke transformation is used to transmit the currents and three-phase voltage from the coordinate of abc to αβc. The imaginary and real instantaneous powers theory is functioning based on time-domain analysis. It makes this effective for processes in the transient regime and steady-state, also for current power system waveforms and generic voltage [32].

The three phases of Clarke transformation are (non-linear/current/voltage load current) as equations (16-18),

$$\begin{bmatrix} v_\alpha \\ v_\beta \end{bmatrix} = \sqrt{\frac{2}{3}} \begin{bmatrix} 1 & -\frac{1}{2} & -\frac{1}{2} \\ 0 & \frac{\sqrt{3}}{2} & -\frac{\sqrt{3}}{2} \end{bmatrix} \begin{bmatrix} v_a \\ v_b \\ v_c \end{bmatrix} \tag{16}$$

$$\begin{bmatrix} i_\alpha \\ i_\beta \end{bmatrix} = \sqrt{\frac{2}{3}} \begin{bmatrix} 1 & -\frac{1}{2} & -\frac{1}{2} \\ 0 & \frac{\sqrt{3}}{2} & -\frac{\sqrt{3}}{2} \end{bmatrix} \begin{bmatrix} i_a \\ i_b \\ i_c \end{bmatrix} \tag{17}$$

$$\begin{bmatrix} i_{l\alpha} \\ i_{l\beta} \end{bmatrix} = \sqrt{\frac{2}{3}} \begin{bmatrix} 1 & -\frac{1}{2} & -\frac{1}{2} \\ 0 & \frac{\sqrt{3}}{2} & -\frac{\sqrt{3}}{2} \end{bmatrix} \begin{bmatrix} i_{la} \\ i_{lb} \\ i_{lc} \end{bmatrix} \tag{18}$$

Then, the equations (19-21) show that the earlier elements, such as currents/voltage in the α-β coordinate, are converted into the d-q coordinate.

$$\begin{bmatrix} v_d \\ v_q \end{bmatrix} = \begin{bmatrix} \cos\theta & \sin\theta \\ -\sin\theta & \cos\theta \end{bmatrix} \begin{bmatrix} v_\alpha \\ v_\beta \end{bmatrix} \tag{19}$$

$$\begin{bmatrix} i_d \\ i_q \end{bmatrix} = \begin{bmatrix} \cos\theta & \sin\theta \\ -\sin\theta & \cos\theta \end{bmatrix} \begin{bmatrix} i_\alpha \\ i_\beta \end{bmatrix} \tag{20}$$

$$\begin{bmatrix} i_{ld} \\ i_{lq} \end{bmatrix} = \begin{bmatrix} \cos\theta & \sin\theta \\ -\sin\theta & \cos\theta \end{bmatrix} \begin{bmatrix} i_{l\alpha} \\ i_{l\beta} \end{bmatrix} \tag{21}$$

Besides, the instant reactive and active powers are supplied to the grid [33] were computed in equations (22) and (23),

$$P = v_d i_d + v_q i_q \tag{22}$$

$$Q = v_d i_q - v_q i_d \tag{23}$$

To ensure the MPPT operation, a BFOA-based robust controller is used to manage a DC-DC converter to ensure the varying climatic situations (temperature and irradiation). Moreover, the SOA technique is applied to assure a productive decoupled control of the PV system output. Furthermore, the PWM inverter injects active and reactive power into the electrical grid for various operating situations. The converter is limited to ensure the effective filtration of non-linear load harmonic current. As a result, the proposed PV system draft can:

- Maximum power is captured from the fluctuating solar energy.
- By using the PWM inverter, the grid gets various active and reactive powers inserted.
- Using the current harmonic filter, rectify the reactive power and upgrade the PQ.

Moreover, the reference P^{ref} power and PVS $P^{\max}$ power are highly helpful in persuading the effective power command P_{eff}^{ref} of the PWM inverter. In addition, the reactive command Q_{eff}^{ref}'s power is verified based on reactive reference, whereas the total system capacity is observed. Subsequently, current references of dq i_d^{ref} and i_q^{ref} are generated by two fuzzy logic controllers. These current commands are added in tandem to attain the active filtering operation with current harmonic dq elements to be filtering (i_{lqh}, i_{ldh}). The $i_d^{\max\ ref}$ and $i_q^{\max\ ref}$ are individually controlled the whole references i_d^{totref} i_q^{totref} to give the intense inverter output current commands in the dq frame [34]. The challenges related to the current references i_d^{totref}

are on the system's overall capability regarding power and the priority block management of disparate operations (active filtering, reactive power compensation, active power generation). The following section explains this strategy in detail.

3.4.1.Active filtering operation

The harmonic currents of non-linear load were identified by using multiple methods. Especially to extract the components of the harmonic current, a Low Pass Filter (LPF) or Selective Pass Band Filter (SPBF) is used. The Frequency domain compensation based on Fourier analysis is often not used as the real-time processing power required is too high [35]. The instantaneous power theory $p-q$ $d-q$ and synchronous detection method are the two classical methods. Here, the current harmonic components in the $d-q$ reference frame are attained using the difference in LPF outputs (components of direct current) and the non-linear load's $d-q$ currents (The entire current is made up of a basic component that is continual in a harmonic part frame and $d-q$ frame).

3.4.2. PV system active and reactive power capabilities and PQ improvement

PV is not only utilized to absorb the full amount of energy from the sun because non-linear loads are integrated into the grid. So that it helps to increase the power efficiency, at this point, to handle the power of the PV system and enhance its quality, the entire capacity of the system power will be established in the plane of PQ inside the attainable limits. It is important to know the potential powers of active and reactive to nullify the overestimation components of the PV system during its control for power generation and power quality improvement in MPPT.

The maximum limit of active power is determined by PVS-rated power and two DC-DC converters of the system. Furthermore, simulation tests were conducted for various active power levels to evaluate the highest reactive power produced at the PWM inverter's output without weakening the DC bus voltage. The reactive power limit delimits the trapezoidal shaded area of the upper edge ($Q^{\max}$). The system's entire potential of reactive power in the PQ plane is determined using energy analysis. Its performance is based on the DC bus voltage energy balance. It is possible to indicate the depositing and returning energy by the DC bus capacitance per cycle. DC bus voltage ripples stage has corresponded to this energy. Then the DC bus voltage fluctuations are provided by the reactive power (due to the inverter's operation based on grid ac voltage, the values are allowed by the inverter). It can be considered as the higher boundary of reactive power ($Q^{\max}$). The DC bus voltage is anchored at a stable and smooth level. The inverter control signal parameters are made efficient using the SOA optimization algorithm, which is explained in the below section.

3.5. SOA-Based Control Signal Parameter Optimization

The proposed system's innovation and mathematical modeling are well explained in this section. Seagulls are the minimum specialized of all the seabirds on our planet from the Laridae family. There are several types of seagulls, each with its mass and length. Seagulls are flesh eaters and eat earthworms, amphibians, reptiles, fish, insects, and so on. The majority of seagulls have white plumage on their bodies. Gulls nest in huge, crowded and noisy colonies. Seagulls are highly intellectual and feeders with highly adaptable species. They produce rainfall sounds by using their feet to tempt small reptiles lurking under the water surface. They consume both fresh and salty water.

Generally, a seagull cannot dive deep inside the water to feed on deeper prey. To find and attack the prey, they used its peculiar skills. They have a remarkable potential for migration and striking characteristics. Seagulls migration is done in search of a rich source of food and sustainable weather condition for breeding. This feature is expressed as follows:

- While migrating, Seagulls fly as a flock; the seagulls starting positions are unique to avoid the clash within them.
- Seagulls often follow the fittest seagull in the group, which is also fit for the migration survival, i.e., if the fitness value is 1 and then the fitness of that bird is low compared to others.
- Other seagulls can choose their initial positions based on the fittest seagull.

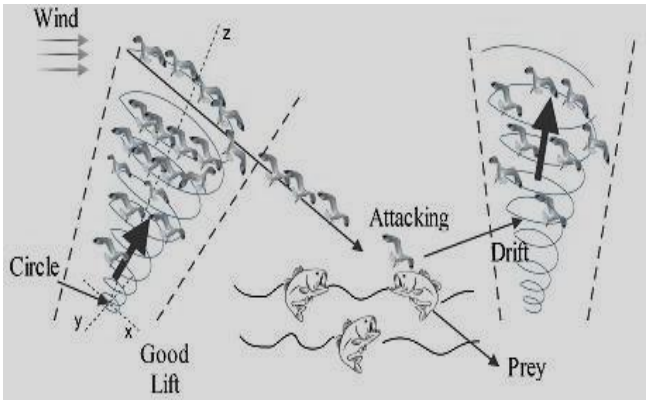

Fig. 3 Flow diagram of the proposed algorithm

Seagulls often attack other migrating birds on their way while they migrate from one location to another. They have expertise in attacking techniques and use natural shape movement while attacking their prey. A conceptual model of these behaviors is illustratedin figure 3. This behavior makes it viable to put together a modern optimization algorithm.

The mathematical models of migration and attacking logic of the prey are the two natural behaviors of seagulls focused on in this paper. This algorithm was developed by moving seagulls' flock from one location to another. Here every seagull must fulfill three constraints:

3.5.1 Avoid collisions

To prevent the collision among neighbors (in-between other seagulls), an extra component A is utilized for the formulation of the search agent's current position, which is given as equation (24),

$$C_s = A \times P_s(x) \tag{24}$$

Where search agent position is denoted as C_s which won't collide with new search agent, denotes the search agent current position, current iteration denotes x, and A indicates the search agents movement behavior, which is computed in equation (25),

$$A = f_c - \left(x \times \left(f_c / iter^{\max}\right)\right)_{x=0,1,\ldots,iter^{\max}} \tag{25}$$

Here, the frequency control of the employed variable A f_c s represented decreased linearly from f_c 0.

3.5.2. Movement in the direction of the best neighbor

After preventing the neighbor's collision, the search agents are moved in the direction of the finest neighbor. It is considered in equation (26),

$$M_s = B \times \left(P_{bs}(x) - P_s(x)\right) \tag{26}$$

Here, P_s approaching the prime fit search agent P_{bs} (i.e., fittest seagull) M_s indicates the search agent's position [36]. The random behavior B is responsible for the actual balance between exploitation and exploration that calculation is given in equation (27),

$$B = 2 \times A^2 \times rand \tag{27}$$

Here $rand$ is a random number within the range of [0, 1].

3.5.3. Remain close to the best search agent

Finally, with regards to the best search agent, the search agent can update its location (equation. 28).

$$D_s = \left|C_s + M_s\right| \tag{28}$$

Therefore, the distance between the best-fit search agent (i.e., the best seagull is selected based on the less fitness value) and the search agent is denoted D_s. Exploitation aims to shaft the history of records and professionalism of the search process. These gulls can continuously alter the approach point while attacking and speed during migration. To sustain the elevation, they use their wings and body weight. The spiral formation performance happens in the air during a prey attack. It happens in x, y z, and planes are defined as equations (29)-(32),

$$x' = r \times \cos(k) \tag{29}$$

$$y' = r \times \sin(k) \tag{30}$$

$$z' = r \times k \tag{31}$$

$$r = u \times e^{kv} \tag{32}$$

Here k is a random number in the range [$0 \le k \le 2\pi$] and r the spiral turn v's radius. And u are the spiral shape's constants, natural logarithm base is e. The renovated place of the search agent is calculated as equation (33),

$$P_s(x) = \left(D_s \times x' \times y' \times z'\right) + P_{bs}(x) \tag{33}$$

The optimal solution is stored $P_s(x)$ here, and the other search agent's location is updated. The proposed SOA begins with a casual generation of the population. During the iteration process, the search agent intercommunicates with each other regarding the position of the best search agent. A is decreased in a straight line from f_c 0. Element B is responsible for the smooth conversion between exploration and exploitation. Hence, exploration and exploitation have excellent potential; SOA considered this a global optimizer.

3.6 *Management of PV system function's priorities*

The ability of the PV system in power terms is distinguished by a maximum current modulus $I^{\max}$ which can be formulated for the cause of limits of the power $P_{\lim}$ and $Q_{\lim}$ is defined as equation (34),

$$I^{\max} = \sqrt{2}\,\frac{\sqrt{P_{\lim}^2 + Q_{\lim}^2}}{3V^{pcc}} \tag{34}$$

Where V^{pcc} is the bus-bar RMS voltage in the PV system active, and are the reactive powers' limits denoted as $P_{\lim}$ $Q_{\lim}$ and for a specified operating point? A rapid reactive power theorem is enacted to limit the power-sharing between the inverter and grid. Using the hysteresis band current control technique, the resultant current of the inverter is different [37]. These are the measured variables capacitor dc voltage, grid voltages, and inverter output currents.

The PV system energy is managed on the basic preference, where it is specified to active power generation over the improvement of power quality. Consequently, the maximum available reactive current value is utilized for harmonic currents mitigation, and reactive power compensation is described in equation (35).

$$I_q^{\max\, ref} = \sqrt{(I^{\max})^2 - (I_d^{\max\, ref})^2} \tag{35}$$

To use the PV system at full capacity in power terms, in this paper, it is suggested to express the overall source for the active power production of the d-q currents, compensation of harmonic mitigation, and reactive power by the equation (36),

$$\left.\begin{aligned} i_d^{totref} &= i_d^{ref} + k_0 i_{dh} \\ i_q^{totref} &= i_q^{ref} + k_0 i_{qh} \end{aligned}\right\} \quad (36)$$

Where k_0 is a positive gain between the range 1 and 0? Then, to reimburse the reactive power over harmonic mitigation, the second preference is provided [38]. The optimized controller is used to limit the resultant current of the inverter. This technique is used to maintain the output current in the permissible zone. So other apparatus does not get affected. Using this system's simulated output, the effectiveness of PQ progress is verified, elaborated in the following section.

4. Results and Discussions

The SOA optimized controller used along with the proposed grid-linked PV system for PQ progress output results is considered in this segment. To design and develop the proposed system along with an optimized controller, MATLAB/SIMULINK is utilized, and that is illustrated in figure 4. The compensation of active and reactive power for the proposed optimized controller is implemented using the voltage and current. The optimized controller is executed to minimize the grid's reactive power integrated with the PV system. The executed controller also stabilizes the dc-link voltage if any PQ problem occurs. Also, it generates controlling pulses to stabilize PQ issues. System limitations are plotted, parameters are decided, and the data are given in table (1). Boundaries like the voltage, current, real power, and reactive power are utilized to evaluate the PQ progress for both the normal and abnormal states. At first, under a normal condition, the capability of the grid-connected PV system is examined to make sure whether the system has any fault on the grid side. For the testing process, the time needed for the simulation is 0–0.2s.

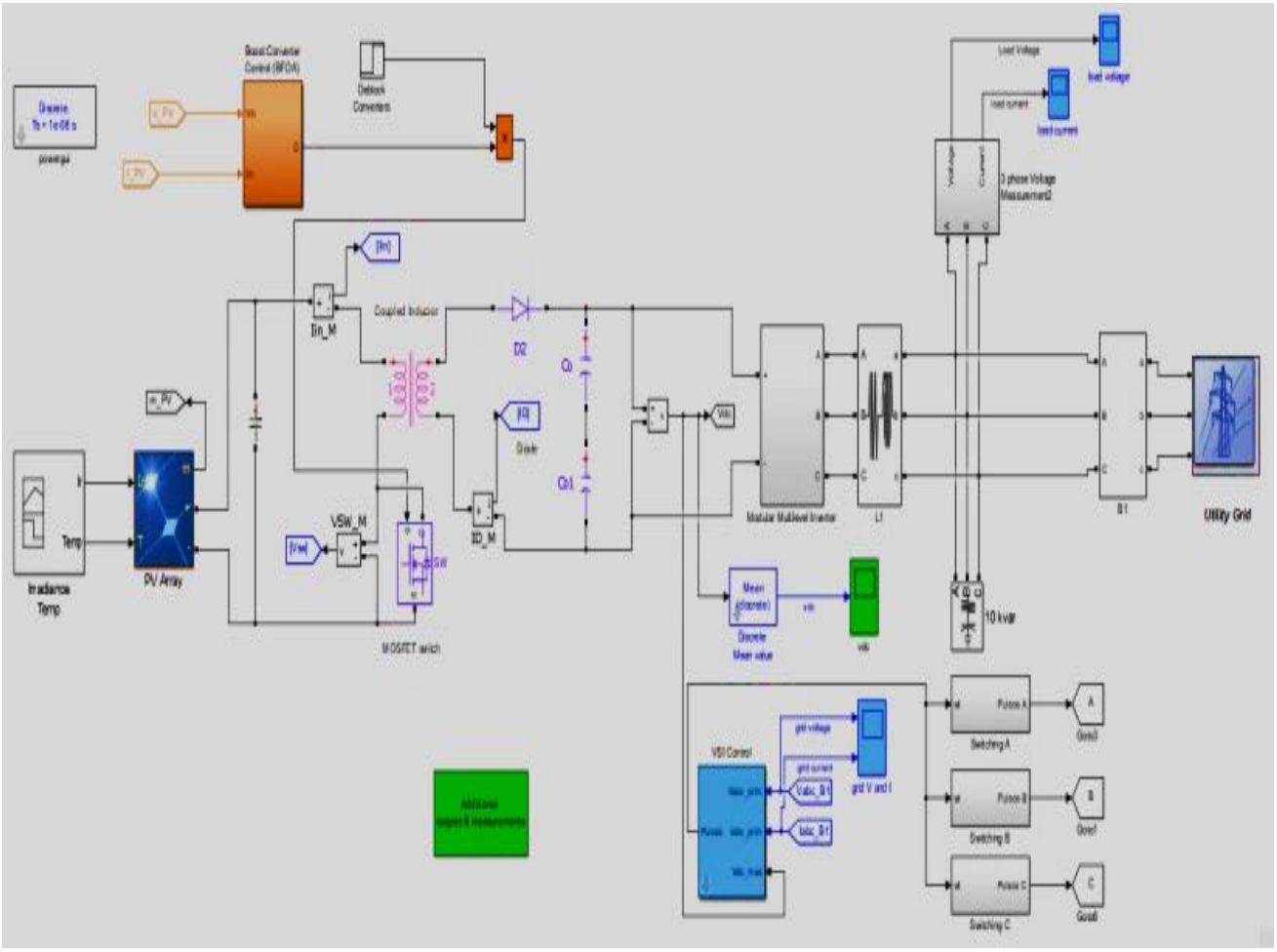

Fig. 4 The Simulink diagram of the proposed grid-connected PV system

Table 1. Implementation parameters

Maximum Power (W)	3.052k
Cells per module (Ncell)	96
Open circuit voltage Voc (V)	64.2
Short-circuit current Isc (A)	5.96
The voltage at maximum power point Vmp (V)	54.7
Current at maximum power, point Imp (A)	5.58
Light-generated current IL (A)	6.0092
Diode saturation current I0 (A)	6.30e-12
Diode ideality factor	0.94504
Shunt resistance Rsh (ohms)	269.5934
Series resistance Rs (ohms)	0.37152
Nominal power and frequency [Pn(VA) fn(Hz)]	[1000 100e3]
Winding1 parameters [V1(Vrms) R1(ohm) L1(H)]	[500 0 0]
Winding 2 parameters [V2(Vrms) R2(ohm) L2(H)]	[500 0 0]
Magnetization resistance and inductance	[Rm(ohm) Lm(H)]
Nominal phase-to-phase voltage Vn (Vrms)	260
Nominal frequency fn (Hz)	60
Cells per module (Ncell)	96
Open circuit voltage Voc (V)	64.2
Short-circuit current Isc (A)	5.96
The voltage at maximum power point Vmp (V)	54.7
Current at maximum power, point Imp (A)	5.58
Light-generated current IL (A)	6.0092

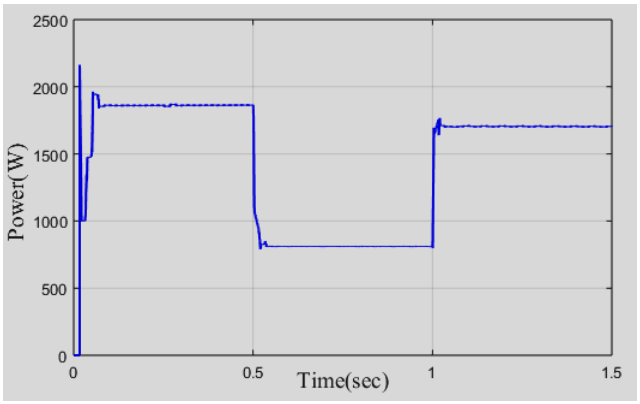

Fig. 5 Analysis of PV irradiance variation level

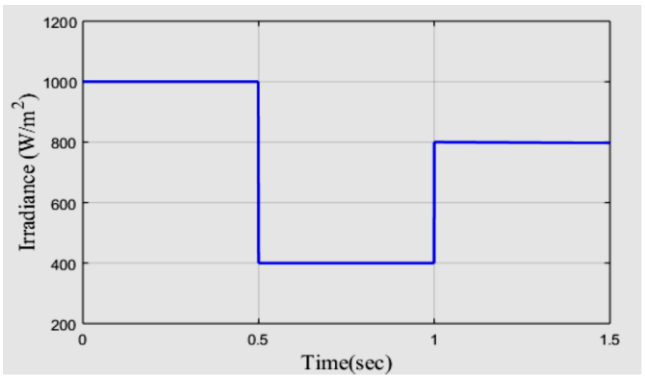

(a)

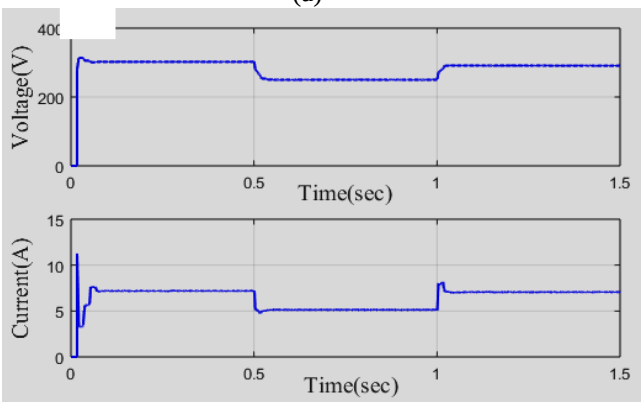

(b)

Fig. 6 Analysis of (a) PV output voltage, current, and (b) power

The input of PV as irradiance is described in figure 5, and it is improved with the help of a DC-DC converter based on the BFOA algorithm. The induced power and the respective voltage and current are described in figure 6, as well as the induced power shifted to the grid by utilizing the VSI and the filter with three-phase. The PQ problems such as voltage fluctuations and interrupt may affect the grid. Based on PQ errors, the outputs are verified using two cases.

Case1: Performance analysis of voltage fluctuations affects the grid

In the first case, a voltage fluctuation affects the grid side, and then a performance analysis is made to analyze the effectiveness. In figure 7, the performance analysis of load voltage and current. Here, under-voltage fluctuations state grid side limitations are expressed in figures 8 & 9. Here, at the time duration of 0.01–0.05s, a PQ error is found. Then the grid voltage amplitude decreased 25% from the initial value, and there was a slight increase in grid current and vice versa. There is an impact on reactive power, and real power of the grid and PQ issues occur at the grid side. Here, various solution techniques are used for solving voltage fluctuations conditions and the PQ magnification.

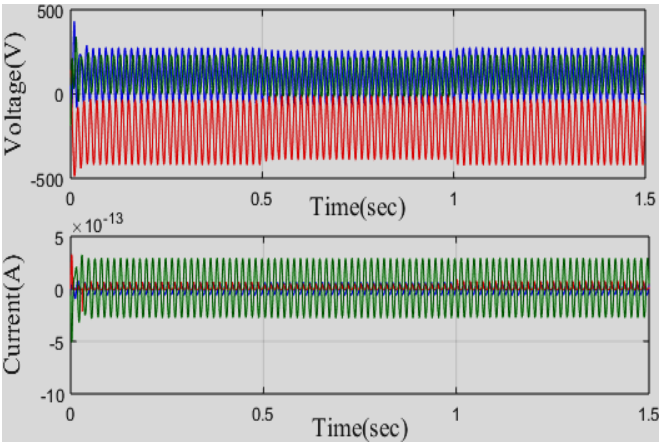

Fig. 7 Performance analysis of load voltage and current in case 1

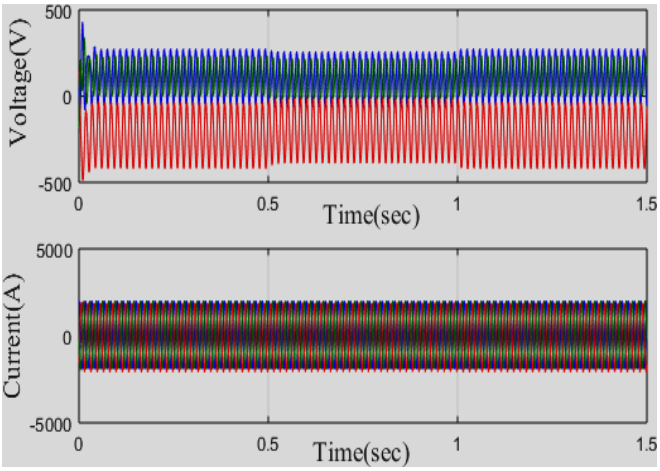

Fig. 8 Performance analysis of Grid voltage and current in case 1

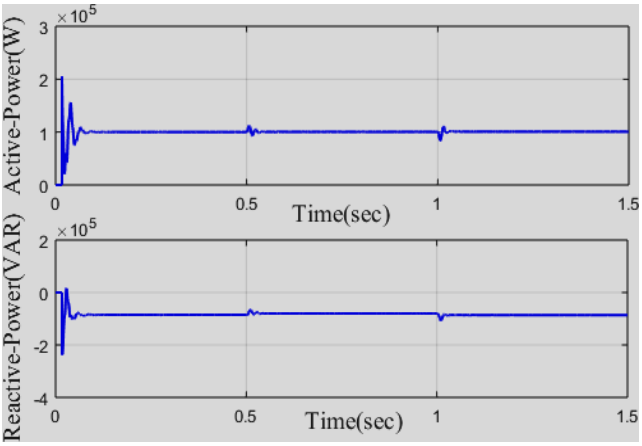

Fig. 9 Performance analysis of Active and reactive power of grid in case 1

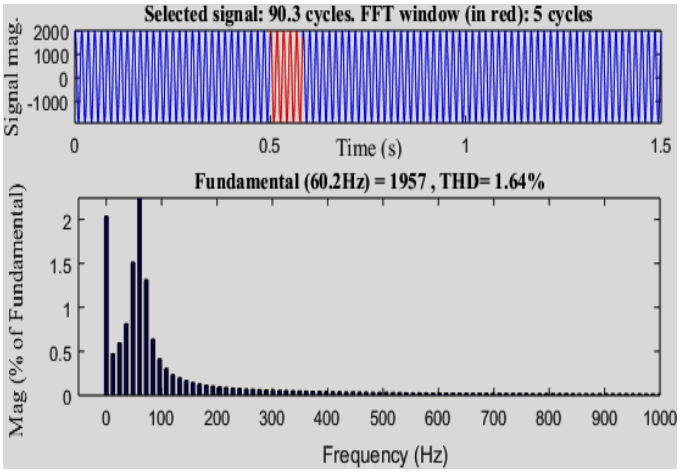

(a)

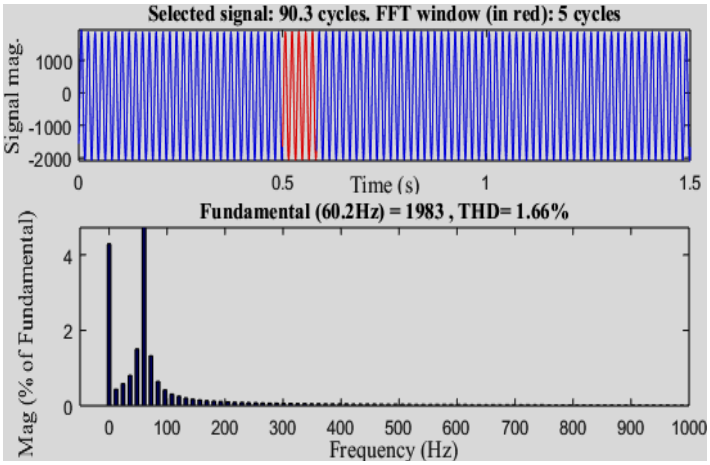

(b)

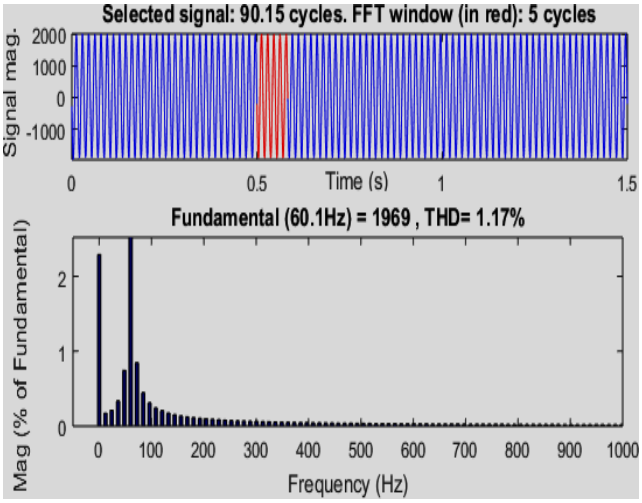

(c)

Fig. 10 Performance of FFT analysis in (a) A-phase, (b) B-phase, and (c) C-phase using proposed controller case 1

During voltage fluctuations, the grid side voltage of the proposed controller is verified using FFT analysis. Also, the affected PQ problem grid is portrayed in figure 10. As per the output of these diagrams, the controller can able to perform unaided active and reactive output power.

Case2: Performance analysis of interrupt-affected grid

During the interrupted grid, the capability analysis of load current and voltage is given in figure 11. Here, in this case, the voltage fluctuations had an impact on the grid side, and in figure 12, the grid's performance analysis of current and voltage throughout the interrupted grid is shown. The problem with grid current, voltage, and active and reactive power has been clarified. In figure 13, the real and reactive power obtained through the interrupted grid is evaluated by using some propound method. Figure 14 shows the grid side voltage during the interrupted grid, which is analyzed using the proposed controller FFT.

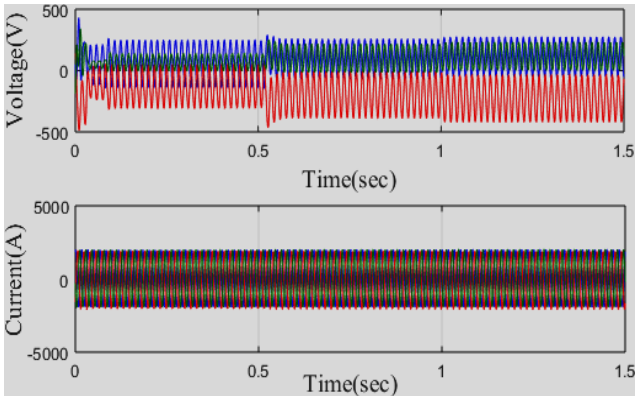

Fig. 11 Performance analysis of load voltage and current in case 2

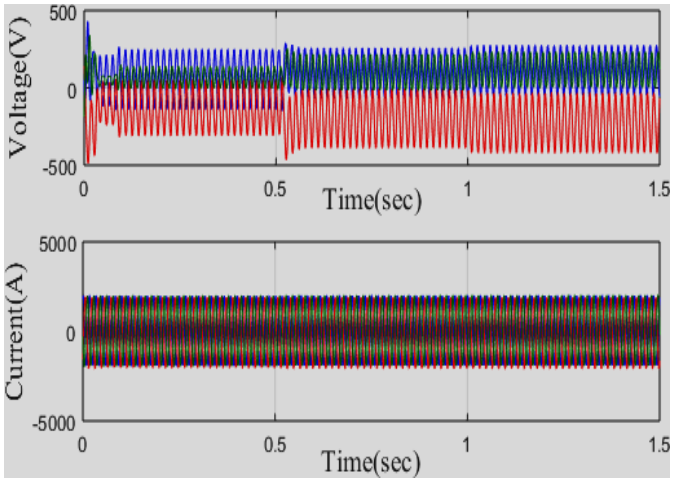

Fig. 12 Performance analysis of Grid voltage and current in case 2

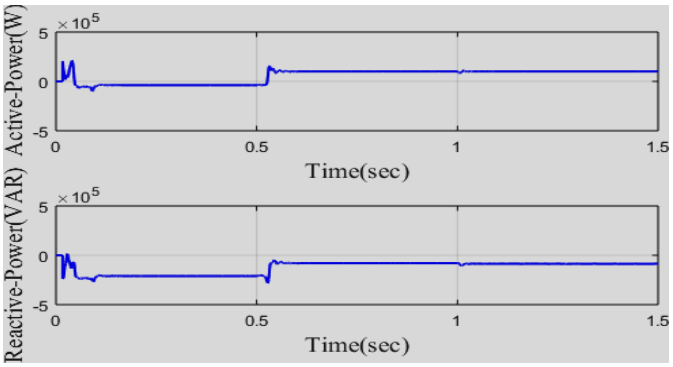

Fig. 13 Performance analysis of grid active and reactive power in case 2

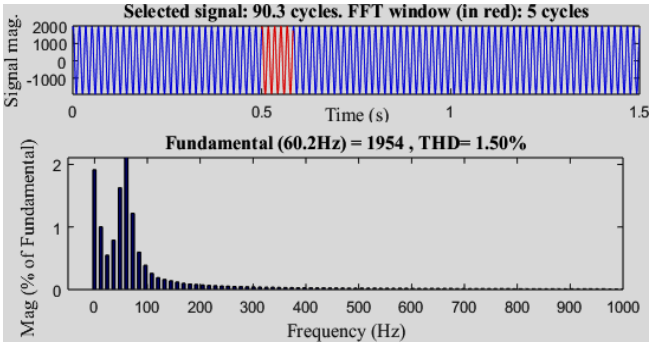

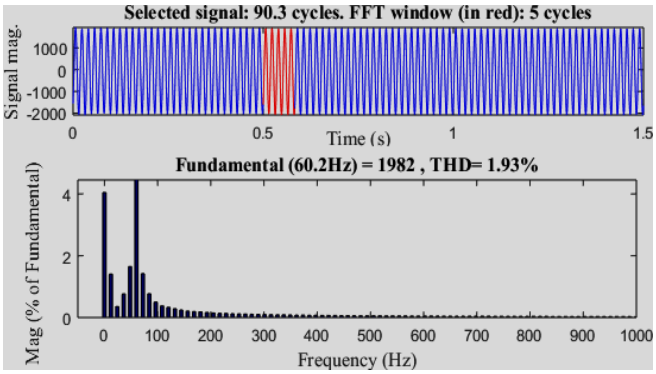

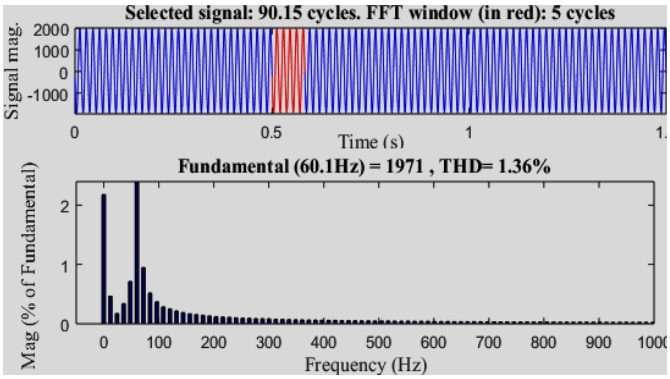

Fig. 14 Performance of FFT analysis in (a) phase A, (b) phase B, and (c) phase C using proposed controller case 2

The comparison analysis of the proposed method can be presented with two different cases, shown in figure 15. The proposed method's comparison analysis proves the system's accuracy and efficiency. The DC link voltage and generated power can be compared with existing and proposed methods. From the graphs, the proposed method efficiency is analyzed with the parameters of rising time, which only meets the reference voltage of the MG structure. The analysis concluded that the proposed method has better results in managing power among the generation and grid sides.

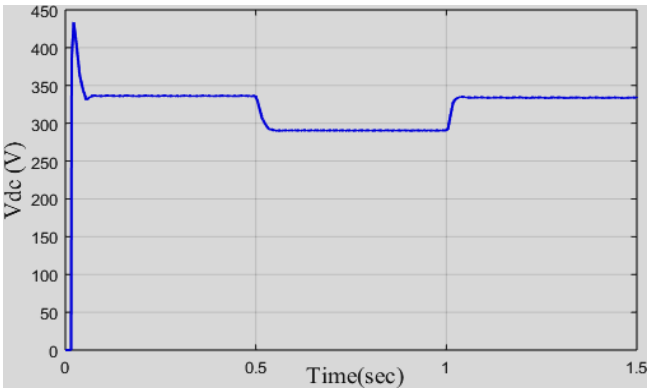

(a)

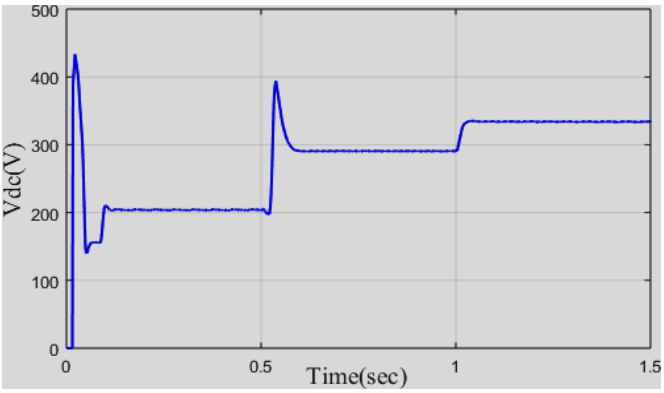

(b)

Fig. 15 The performance analysis of DC-link voltage (a) Case 1 and (b) Case 2

The THD analysis of the Grid side voltage in figure 16 uses different cases. According to this evaluation, harmonics are significantly minimized in the lower order. Even though the THD voltage is minimized, it is preferable in other applications. Various techniques are used in figure 17, indicating harmonic analysis of the Grid sidevoltage.

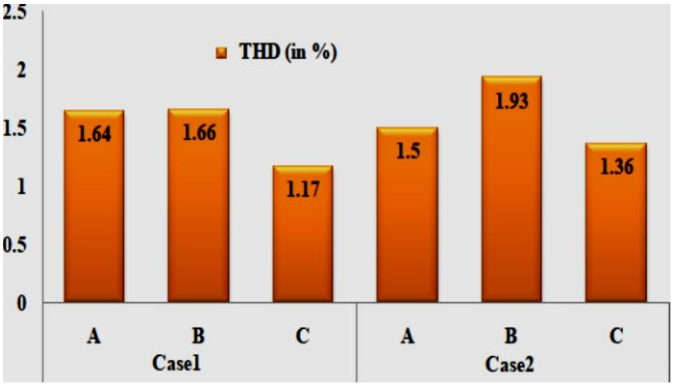

Fig. 16 THD analysis of grid current in different Cases

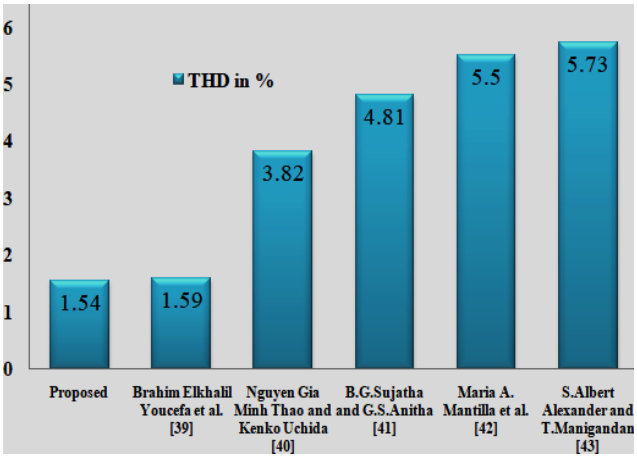

Fig. 17 THD comparison analysis of grid voltage in different controller

Table 2. Comparison analysis of the proposed methodology (THD)

Sl. No	Methods	3rd harmonic	5th harmonic	7th harmonic
1	Proposed	10.25	9.474	7.58
2	AOA	22.45	10.54	10.22
3	GO	18.54	15.9	14.35
4	GSA	15.65	13.12	12.12
5	GA	11.02	10.98	10.55

Sl. No	Methods	11th harmonic	13th harmonic	17th harmonic
1	Proposed	6.54	3.21	14
2	AOA	10.35	10.37	11.01
3	GO	14.12	14.05	13.89
4	GSA	13.65	10.21	10.32
5	GA	10.38	10.32	10.01

Table 3. Comparison analysis of the proposed methodology

Sl. No	Methods	Power (3.05kW)
1	Proposed	3.0415
2	AOA	2.9845
3	GO	2.7518
4	GSA	2.3812
5	GA	2.0089

The effectiveness of the proposed technique based on comparison analysis is given in detail. As for the harmonic analysis, the comparative analysis of the proposed methodis efficiently analyzed and verified.

4. Conclusion

The power quality (PQ) enhancement is ensured by implementing the three-phase grid-connected PV system on an SOA-based active and reactive power controller. The platforms like MATLAB/SIMULINK are used for designing the proposed system, and with the help of some dummy results, the existing controllers are verified. Using various time instants, the problems with PQ are decided, and the behavior is examined. Here, two prime controllers are used. (1) To trace the greatest powers through the PV panels and boost DC/DC converter, the BFOA optimized MPPT controller is used. (2) The SOA optimized controller for the grid-integrated three-phase inverter is used to optimize the control signal parameters. The active and reactive powers are managed by limiting the pulses of the three-phase modular multilevel inverter. Depending on the FFT analysis and simulated output, the THD performance, reactive power compensation, and maximum power concurrently produced are obtained via the PV array of the grid.

Acknowledgements

I thank my supervisor Dr. Puttamadappa C, and Dr. Y L Chandrashekar, who made the work possible. His guidance and advice boosted my research in all the uncertainty.

Finally, an individual thanks all my family members for their continuous support towards the journey in research.

References

[1] H.Jafarian, R.Cox, J.H. Enslin, S.Bhowmik and B.Parkhideh, "Decentralized Active and Reactive Power Control for an AC-Stacked PV Inverter With Single Member Phase Compensation," IEEE Transactions on Industry Applications, vol.54, no.1, pp.345-355, 2018

[2] S.Jain, M.B.Shadmand and R.S.Balog, "Decoupled Active and Reactive Power Predictive Control for PV Applications Using a Grid-Tied Quasi-Z-Source Inverter," IEEE Journal of Emerging and Selected Topics in Power Electronics, vol.6, no.4, pp.1769-1782, 2018

[3] Vinit Kumar and Mukesh Singh, "Sensorless DC-link control approach for three-phase grid integrated PV system," Electrical Power and Energy Systems, Vol.112, pp.309–318, 2019

[4] Abdelbaset Laib, Fateh Krim, Billel Talbi and Abdeslem Sahli, "A Predictive Control Scheme for Large- Scale Grid-Connected PV System Using High- Level NPC Inverter," Arabian Journal for Science and Engineering, Vol.45, pp.1685–1701, 2020

[5] J.Zhang, "Unified control of Z-source grid-connected photovoltaic system with reactive power compensation and harmonics restraint: design and application," IET Renewable Power Generation, vol.12, no.4, pp.422-429, 2018

[6] Yonghao Gui, Gil Ha Lee, Chunghun Kim, and Chung Choo Chung, "Direct power control of grid-connected voltage source inverters using port-controlled Hamiltonian system," International Journal of Control, Automation and Systems, vol.15, pp.2053–2062, 2017

[7] Ahmed A.S.Mohamed, Hamid Metwally, Ahmed El-Sayed, and SI.Selem, "Predictive neural network based adaptive controller for grid-connected PV systems supplying pulse-load," SolarEnergy, Vol.193, pp.139–147, 2019

[8] Hua Li, Che Wen, Kuei-Hsiang Chao, and Ling-Ling Li, "Research on Inverter Integrated Reactive Power Control Strategy in the Grid-Connected PV Systems," Energies, Vol.10, pp.1-21, 2017

[9] P.Shukl and B.Singh, "Delta-Bar-Delta Neural-Network-Based Control Approach for Power Quality Improvement of Solar-PV-Interfaced Distribution System," IEEE Transactions onIndustrial Informatics, vol.16, no.2, pp.790-801, 2020

[10] Seyyed Ali Akbar Fallahzadeh, Navid Reza Abjadi and Abbas Kargar, "Decoupled Active and Reactive Power Control of a Grid-Connected Inverter-Based DG Using Adaptive Input– Output Feedback Linearization," Iranian Journal of Science and Technology, Transactions of Electrical Engineering, Vol.44, pp.1369–1378, 2020

[11] R.K.Varma, S.A.Rahman, and T.Vanderheide, "New Control of PV Solar Farm as STATCOM (PV-STATCOM) for Increasing Grid Power Transmission Limits During Night and Day," IEEE Transactions on Power Delivery, vol.30, no.2, pp.755-763, 2015

[12] Lucas S.Xavier, Allan F.Cupertino, Jose T.de Resende, Victor F.Mendes and Heverton A.Pereira, "Adaptive current control strategy for harmonic compensation in single-phase solar inverters," Electric Power Systems Research, Vol.142, pp.84–95, 2017

[13] K.Palanisamy, D.P.Kothari, Mahesh K.Mishra, S.Meikandashivam, and I.Jacob Raglend, "Effective utilization of unified power quality conditioner for interconnecting PV modules with grid using power angle control method," Electrical Power and Energy Systems, Vol.48, pp.131–138, 2013

[14] F.Lin, K.Lu, and B.Yang, "Recurrent Fuzzy Cerebellar Model Articulation Neural Network Based Power Control of a Single-Stage Three-Phase Grid-Connected Photovoltaic System During Grid Faults," IEEE Transactions on Industrial Electronics, vol.64, no.2, pp.1258-1268, 2017

[15] T.Sreekanth, N.Lakshminarasamma, and M.K.Mishra, "Grid tied single-stage inverter for low- voltage PV systems with reactive power control," IET Power Electronics, vol.11, no.11,pp.1766-1773, 2018

[16] Vijaya Huchche, Prachi Salodkar and Pratik Manusmare, "Reactive Power Compensation of the Grid Connected PV System," Helix, Vol.9, No.6, pp.5836-5840, 2019

[17] Ameerul A.J.Jeman, Naeem M S Hannoon, Nabil Hidayat, Mohamed M.H.Adam, Ismail Musirin, and Vijayakumar. V, "Active and reactive power management of grid connected photovoltaic system," Indonesian Journal of Electrical Engineering and Computer Science, Vol.13, No.3, pp.1324-1331, 2019

[18] Hanan A.Mosalam, Ragab A.Amer, and G.A.Morsy, "Fuzzy logic control for a grid-connected PV array through Z-source-inverter using maximum constant boost control method," Ain Shams Engineering Journal, Vol.9, pp.2931–2941, 2018

[19] W.Liang, Y.Liu, and J.Peng, "A Day and Night Operational Quasi-Z Source Multilevel Grid- Tied PV Power System to Achieve Active and Reactive Power Control," IEEE Transactionson Power Electronics, vol.36, no.1, pp.474-492, 2021

[20] B.Gayathri Devi and B.K.Keshavan, "A novel hybrid Phase Shifted-Modified Synchronous Optimal Pulse Width Modulation based 27-level inverter for grid-connected PV system",Energy, Vol.178, pp.309-317, 2019

[21] Muhammad Talha, SRS.Raihan and N.Abd Rahim, "PV inverter with decoupled active and reactive power control to mitigate grid faults," Renewable Energy, Vol.162, pp.877-892, 2020

[22] Muammar Zainuddin, Frengki Eka Putra Surusa, Syafaruddin, and Salama Manjang, "Constant Power Factor Mode of Grid-Connected Photovoltaic Inverter for Harmonics Distortion Assessment," International Journal of Renewable Energy Research, Vol.10, No.3, pp.1525- 1535, 2020

[23] J.Preetha Roselyn, C.Pranav Chandran, C.Nithya, D.Devaraj, R.Venkatesan, Varun Gopal and Sai Madhura, "Design and implementation of fuzzy logic-based modified real-reactive power control of inverter for low voltage ride through enhancement in grid-connected solar PV system," Control Engineering Practice, Vol.101, 2020

[24] Manash Kumar Mishra and Vivek Nandan Lal, "An improved methodology for reactive power management in grid integrated solar PV system with maximum power point condition," SolarEnergy, Vol.199, pp.230–245, 2020

[25] Insu Kim and Ronald G.Harley, "Examination of the effect of the reactive power control of photovoltaic systems on electric power grids and the development of a voltage-regulation method that considers feeder impedance sensitivity," Electric Power Systems Research, Vol.180, 2020

[26] Boualem Boukezata, Abdelmadjid Chaoui, Jean-Paul Gaubert and Mabrouk Hachemi, "Power Quality Improvement by an Active Power Filter in Grid-connected Photovoltaic Systems with Optimized Direct Power Control Strategy", Electric Power Components and Systems, Vol.44, No.18, pp.2036-2047, 2016.

[27] Belkacem Belabbas, Tayeb Allaoui, Mohamed Tadjine, and Mouloud Denai, "Power management and control strategies for off-grid hybrid power systems with renewable energies and storage," Energy Systems, Vol.10, pp.355–384, 2019.

[28] Ho-sung Kim, Jong-Hyun Kim, Byung-Duk Min, Dong-Wook Yoo, and Hee-Je Kim, "A highly efficient PV system using a series connection of DC–DC converter output with a photovoltaic panel," Renewable Energy, Vol.34, pp.2432–2436, 2009.

[29] K.Sathish Kumar and T.Jayabarathi, "Power system reconfiguration and loss minimization for an distribution systems using bacterial foraging optimization algorithm," Electrical Power andEnergy Systems, Vol.36, pp.13–17, 2012

[30] S.Devi and M.Geethanjali, "Application of Modified Bacterial Foraging Optimization algorithm for optimal placement and sizing of Distributed Generation," Expert Systems withApplications, Vol.41, pp.2772–2781, 2014

[31] Ivan Todorovic, Stevan Grabic and Zoran Ivanovic, "Grid-connected converter active and reactive power production maximization with respect to current limitations during grid faults,"Electrical Power and Energy Systems, Vol.101, pp.311–322, 2018 Hossein Dehghani Tafti, Ali Iftekhar Maswood, Georgios Konstantinou, Josep Pou and Pablo Acuna, "Active/reactive power control of photovoltaic grid-tied inverters with peak current limitation and zero active power oscillation during unbalanced voltage sags," IET Power Electronics, Vol.11, No.6, pp.1066-1073, 2018

[32] Bouazza Fekkak, Mohamed Menaa, and Bouziane Boussahoua, "Control of transformer less grid-connected PV system using average models of power electronics converters withMATLAB/Simulink," Solar Energy, Vol.173, pp.804–813, 2018

[33] M.Boutoubat, L.Mokrani and M.Machmoum, "Control of a wind energy conversion system equipped by a DFIG for active power generation and power quality improvement," RenewableEnergy, Vol.50, pp.378-386, 2013

[34] Gaurav Dhiman, Krishna Kant Singh, Adam Slowik, Victor Chang, Ali Riza Yildiz, Amandeep Kaur, and Meenakshi Garg, "EMoSOA: a new evolutionary multi‐ objective seagull optimization algorithm for global optimization," International Journal of Machine Learning and Cybernetics, Vol.12, pp.571–596, 2021

[35] H. Jia, Z. Xing and W. Song, "A New Hybrid Seagull Optimization Algorithm for Feature Selection," IEEE Access, Vol.7, pp.49614-49631, 2019.

[36] Pradipta Kumar Sahoo, Pravat Kumar Ray and Pranati Das, "Active and reactive power control of three phase grid connected PV system," Smart Grid and Green Communications, Vol.1, No.4, pp.275-291, 2018

[37] Atallah Ouai, Lakhdar Mokrani, Mohamed Machmoum, and Azeddine Houari, "Control and energy management of a large scale grid-connected PV system for power qualityimprovement," Solar Energy, Vol.171, pp.893–906, 2018

[38] Brahim Elkhalil Youcefa, Ahmed Massoum, Said Barkat and Patrice Wira, "Backstepping Predictive Direct Power Control of GridConnected Photovoltaic System Considering PowerQuality Issue", Majlesi Journal of Electrical Engineering, Vol.14, No.1, pp.9-23, 2020

[39] Nguyen Gia Minh Thao and Kenko Uchida, "Active And Reactive Power Control Techniques Based On Feedback Linearization And Fuzzy Logic For Three-Phase Grid-ConnectedPhotovoltaic Inverters", Asian Journal of Control, Vol.17, No.5, pp.1–25, 2015

[40] B.G.Sujatha and G.S.Anitha, "Enhancement of PQ in grid connected PV system using hybrid technique", Ain Shams Engineering Journal, Vol.9, No.4, pp.869-881, 2018

[41] Maria A. Mantilla, Johann F. Petit and Gabriel Ordonez, "Control of multi-functional grid- connected PV systems with load compensation under distorted and unbalanced grid voltages",Electric Power Systems Research, Vol.192, 2021

[42] S.Albert Alexander and T.Manigandan, "Power quality improvement in solar photovoltaic system to reduce harmonic distortions using intelligent techniques", Journal of Renewable andSustainable Energy, Vol.6, 20